Supporting Information

An Arsenite-Loaded Albumin Nanoparticle for Targeted Synergistic Chemo-Photothermal Therapy of HCC

Ke Zhang[a^], Dan Li[a^], Bin Zhou[a^], Jiani Liu[a], Xiangjie Luo[b], Ruixue Wei[c], Lizhu Wang[a], Xiaojun Hu[a], Zhongzhen Su[a,*], Hongyu Lin[b,*] , Jinhao Gao[b,*], Hong Shan[a,*]

[a] Department of Interventional Medicine, Department of Ultrasound, Guangdong Provincial Key Laboratory of Biomedical Imaging, Guangdong Provincial Engineering Research Center of Molecular Imaging, The Fifth Affiliated Hospital, Sun Yat-sen University, Zhuhai, Guangdong 519000, China

[b] State Key Laboratory of Physical Chemistry of Solid Surfaces, The MOE Laboratory of Spectrochemical Analysis & Instrumentation, The Key Laboratory for Chemical Biology of Fujian Province, and Department of Chemical Biology, College of Chemistry and Chemical Engineering, Xiamen University, Xiamen 361005, China

[c] Department of Cerebrovascular Diseases, The Second Affiliated Hospital of Zhengzhou University, Zhengzhou, Henan 450052, China

^ Equal contribution

* corresponding authors

E-mail addresses: suzhzh3@mail.sysu.edu.cn (Z. Su), hylin007@xmu.edu.cn (H. Lin), jhgao@xmu.edu.cn (J. Gao), shanhong@mail.sysu.edu.cn (H. Shan).

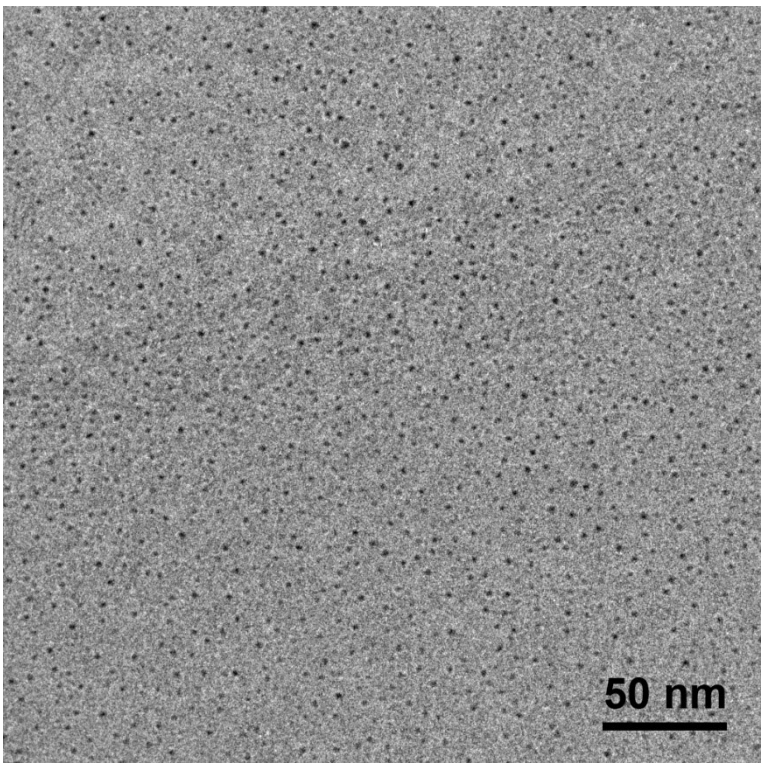

Figure S1. A TEM image of FeAs/HSA.

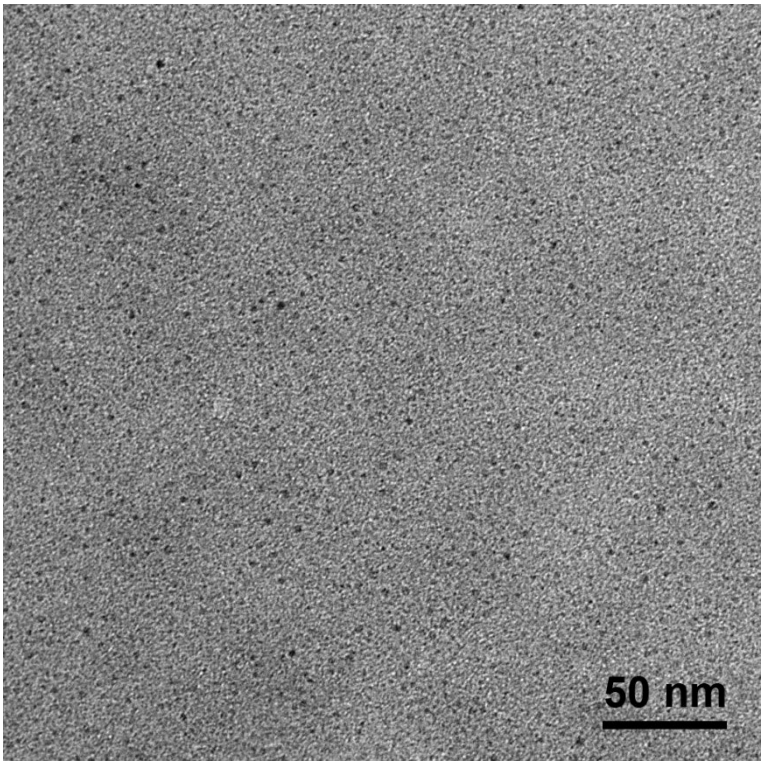

Figure S2. A TEM image of MnAs/HSA.

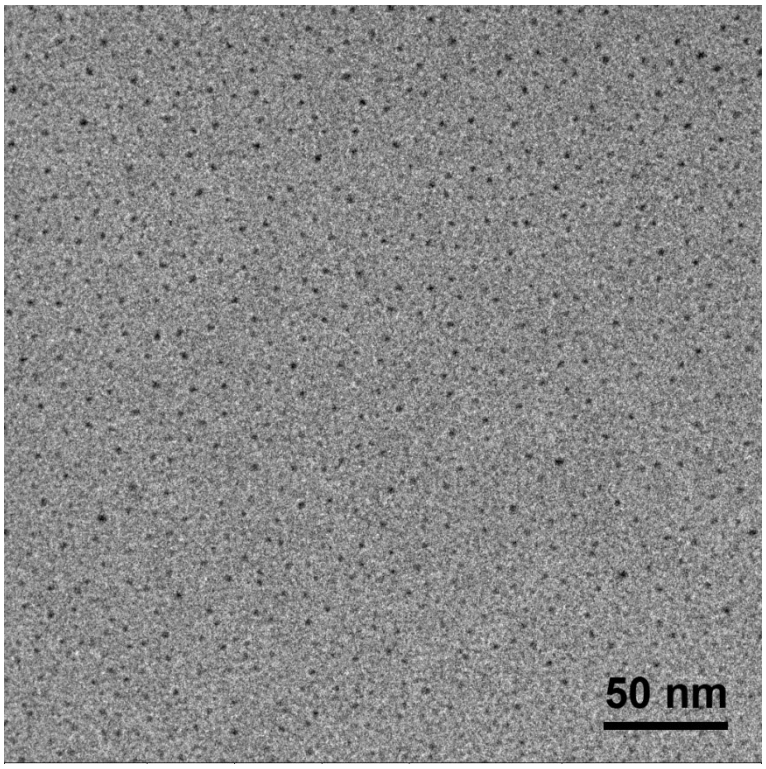

Figure S3. A TEM image of ZnAs/HSA.

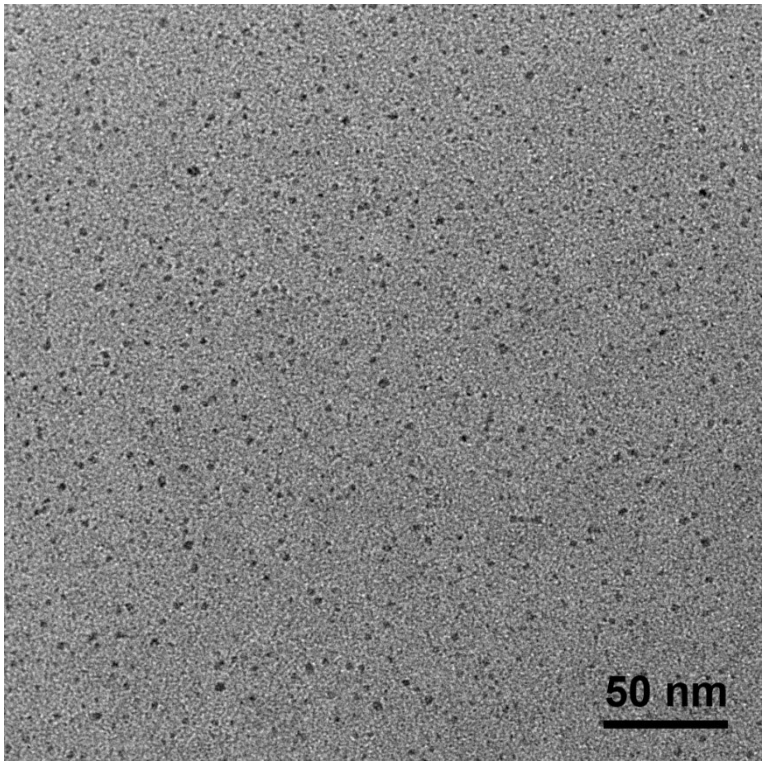

Figure S4. A TEM image of NiAs/HSA.

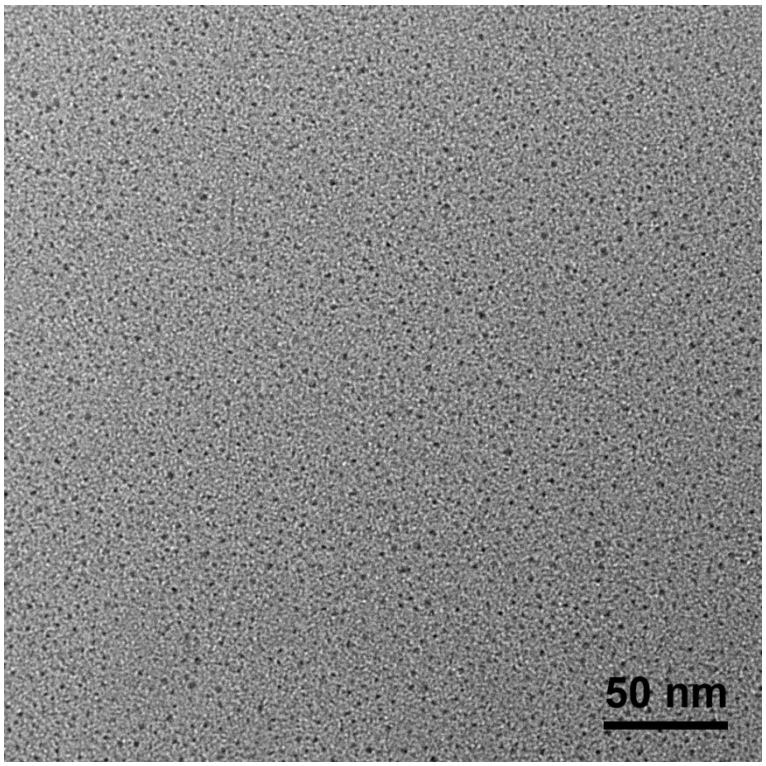

Figure S5. A TEM image of GdAs/HSA.

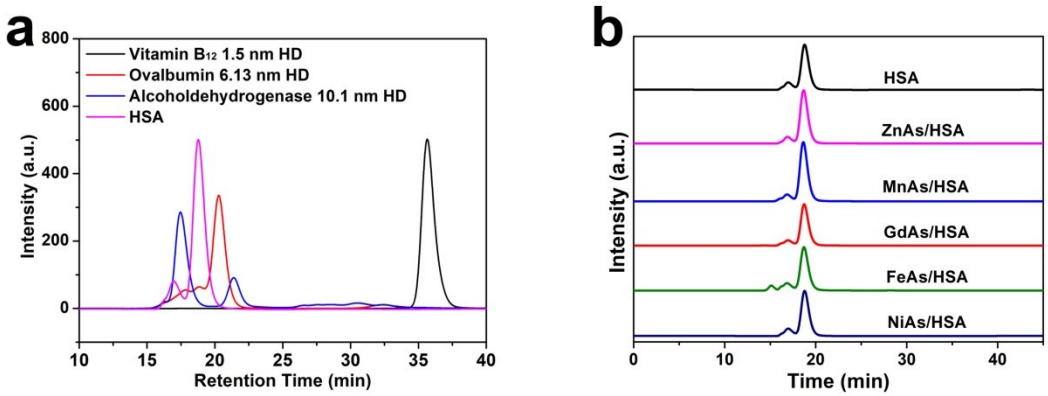

Figure S6. (a) Gel-filtration chromatography (GFC) profiles and hydrodynamic diameters (HDs) of various markers. (b) GFC profiles of indicated nanoparticles after 24 h incubation in 1×PBS buffer containing 10% FBS.

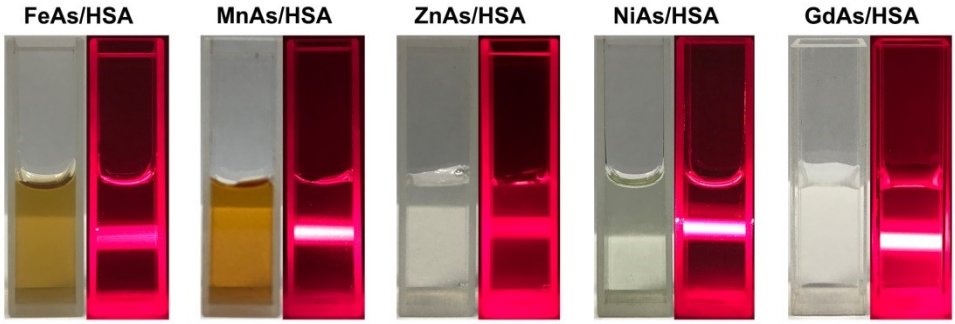

Figure S7. Optical images and Tyndall phenomenon of nanoparticles water dispersion.

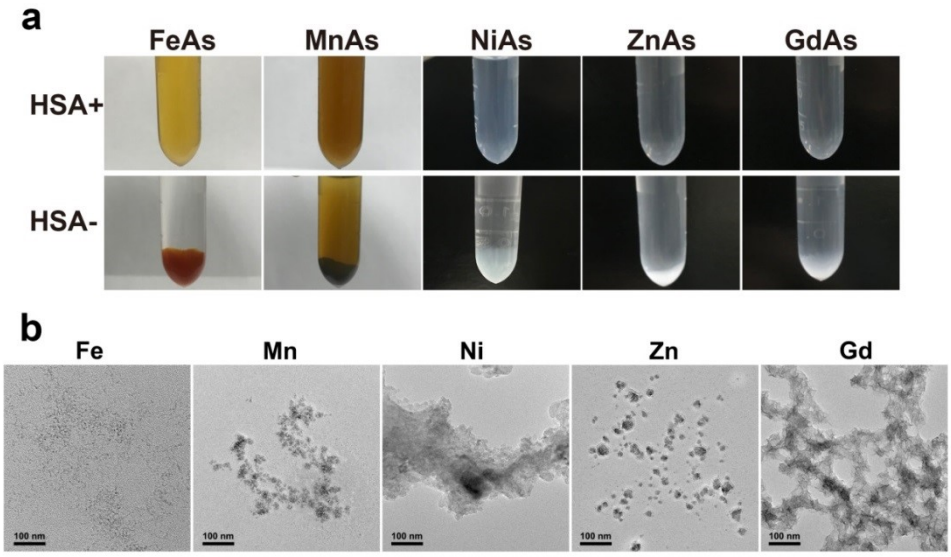

Figure S8. (a) Optical images of nanocomplexes synthesized with HSA (top) or without HSA (bottom) as a template. (b) TEM images of nanocomplexes synthesized without HSA as a template.

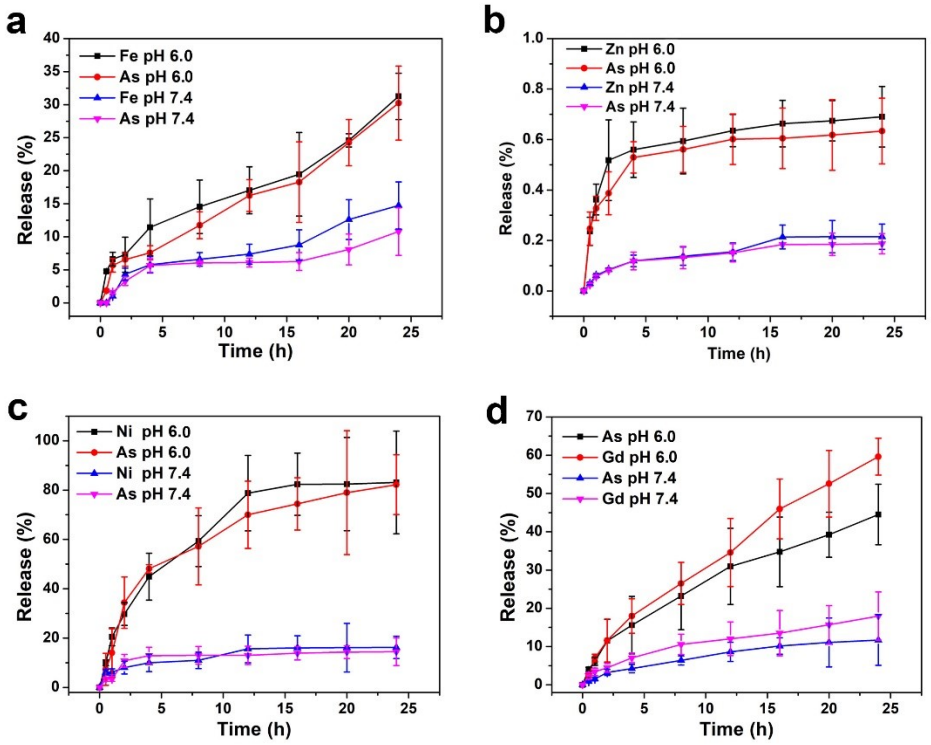

Figure S9. Release profiles of (a) FeAs/HSA, (b) NiAs/HSA, (c) ZnAs/HSA, and (d) GdAs/HSA in 1×PBS buffers at pH 6.0 and 7.4.

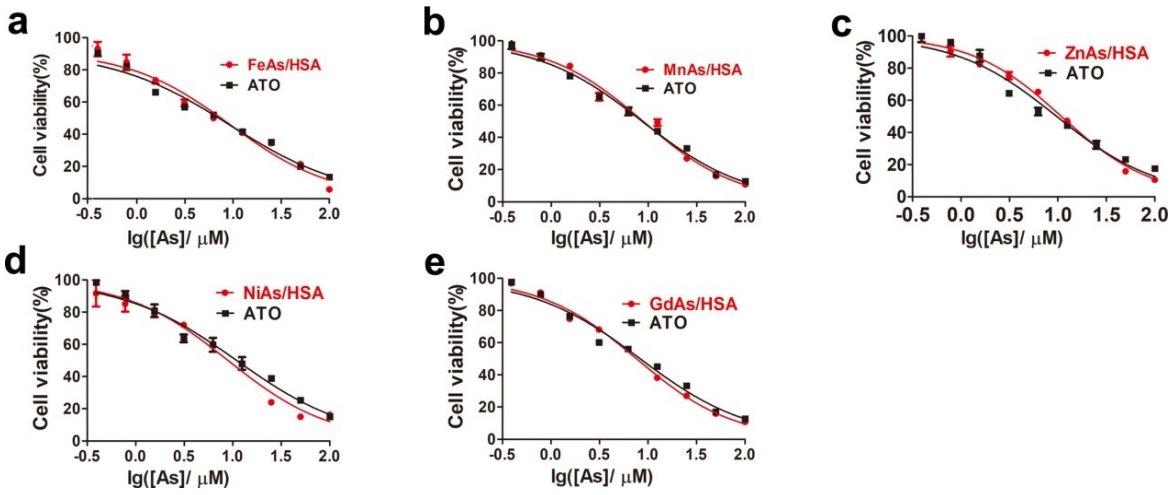

Figure S10. In vitro cytotoxicity assay. SMMC-7721 cells treated with (a) FeAs/HSA, (b) MnAs/HSA, (c) ZnAs/HSA, (d) NiAs/HSA, and (e) GdAs/HSA for 48 h (n = 5/group). ATO was used as a control.

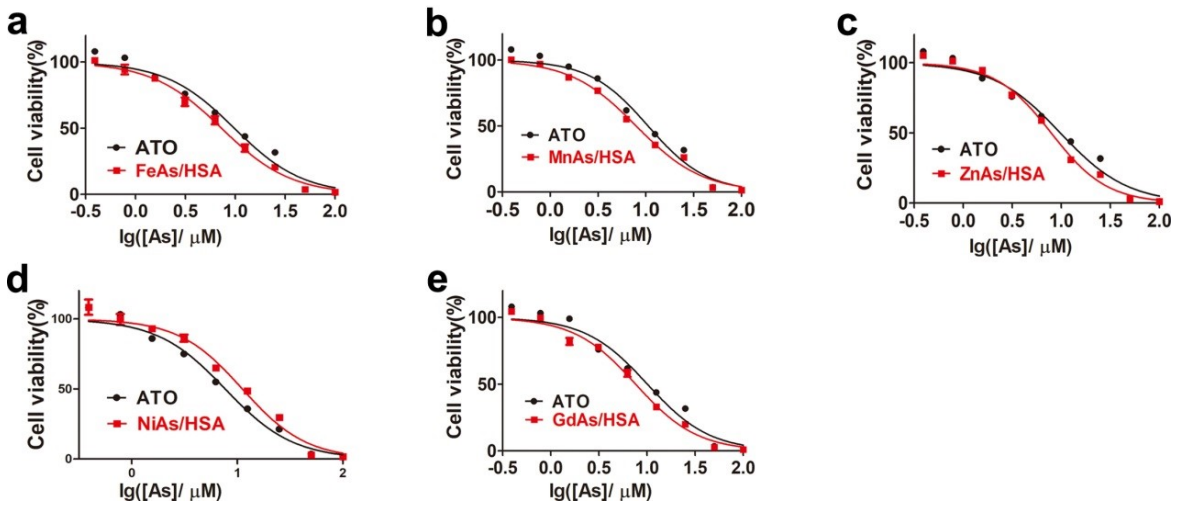

Figure S11. Cytotoxicity of (a) FeAs/HSA, (b) MnAs/HSA, (c) ZnAs/HSA, (d) NiAs/HSA, and (e) GdAs/HSA against Huh7 cells (n = 5/group). ATO was used as a control.

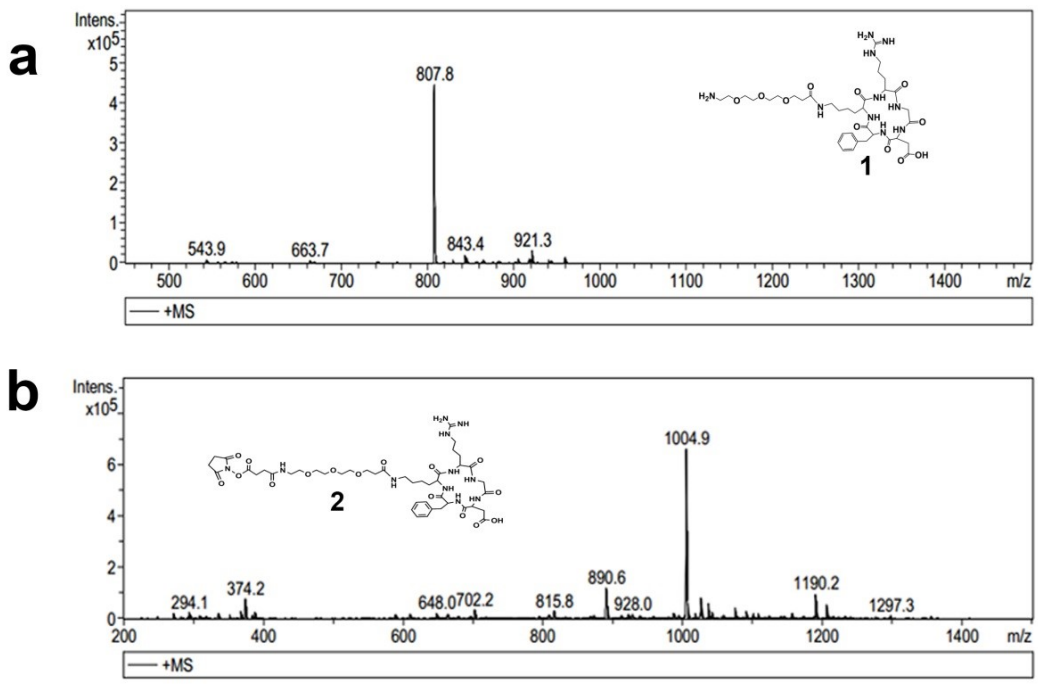

Figure S12. ESI-MS spectra of (a) **1** and (b)**2**.

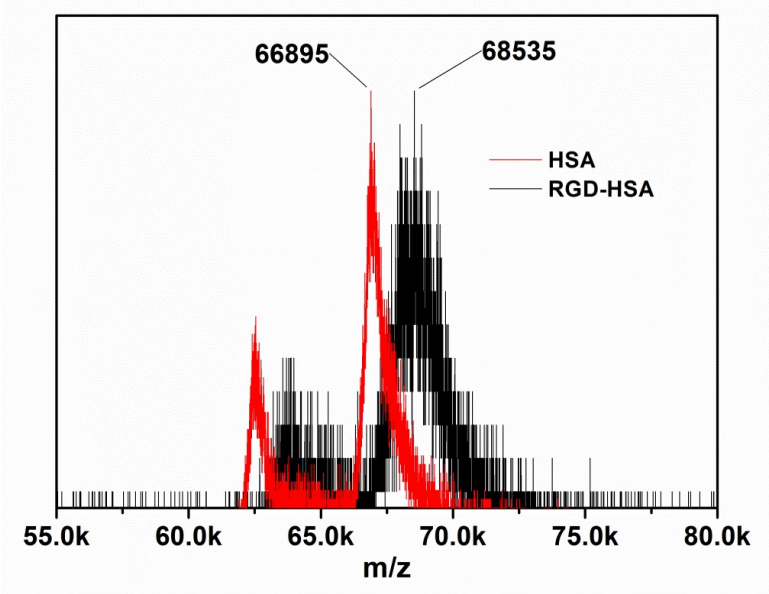

Figure S13. Matrix-assisted laser desorption/ionization time-of-flight (MALDI-TOF) mass spectra of HSA (red) and HSA-RGD (black).

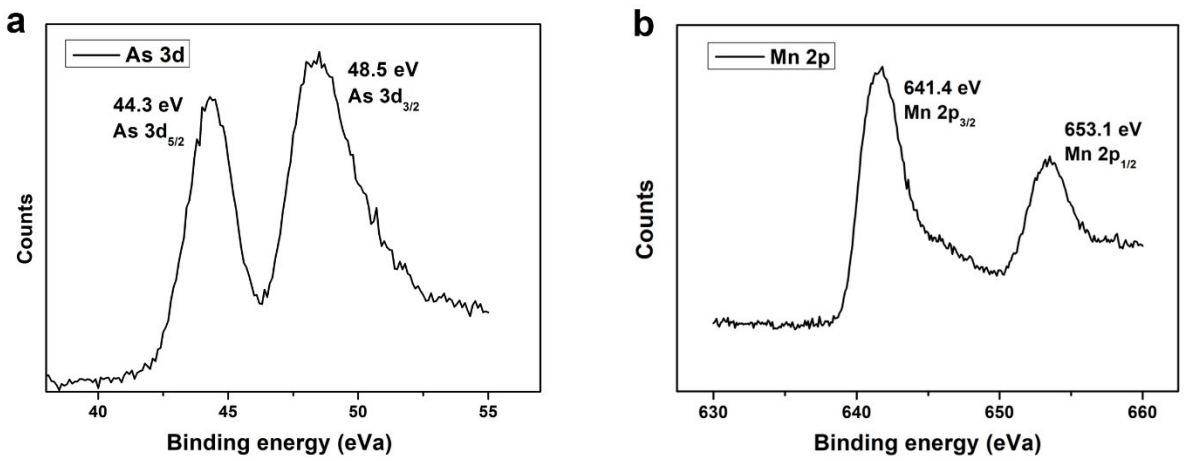

Figure S14. X-ray photoelectron spectroscopy (XPS) spectra of MnAs/HSA-RGD. (a) The peaks of As $3d_{5/2}$ and $3d_{3/2}$ were around 44.3 eV and 48.5 eV, respectively. (b) The peaks of Mn $2p_{3/2}$ and Mn $2p_{1/2}$ were around 641.4 eV and 653.1 eV, respectively.

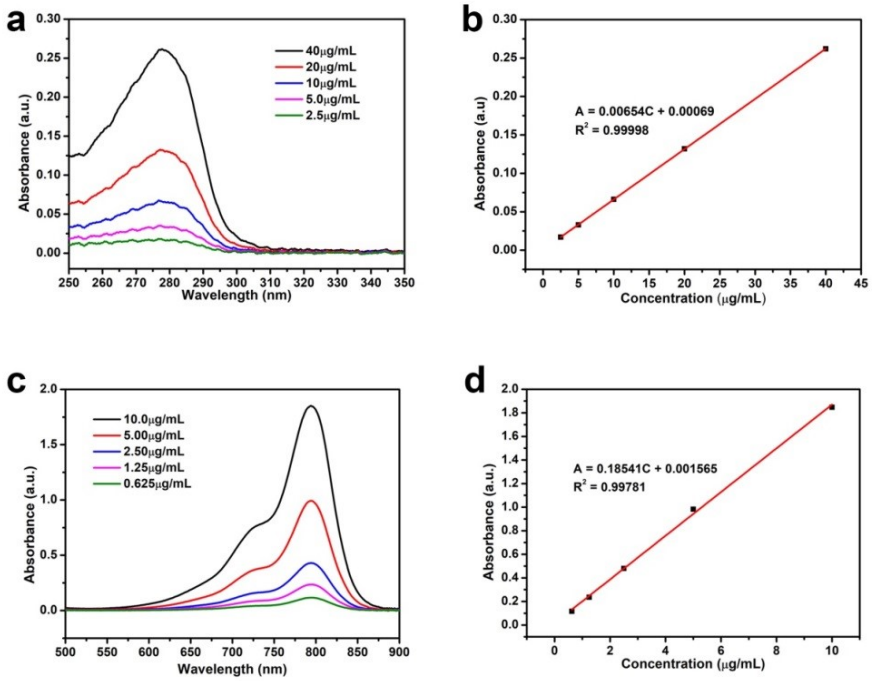

Figure S15. UV/Vis absorbance spectra of (a) HSA and (c) ICG at different concentrations. Corresponding absorbance *vs*. concentration calibration curves for (b) HSA (absorbance at 280 nm) and (d) ICG (absorbance at 760 nm).

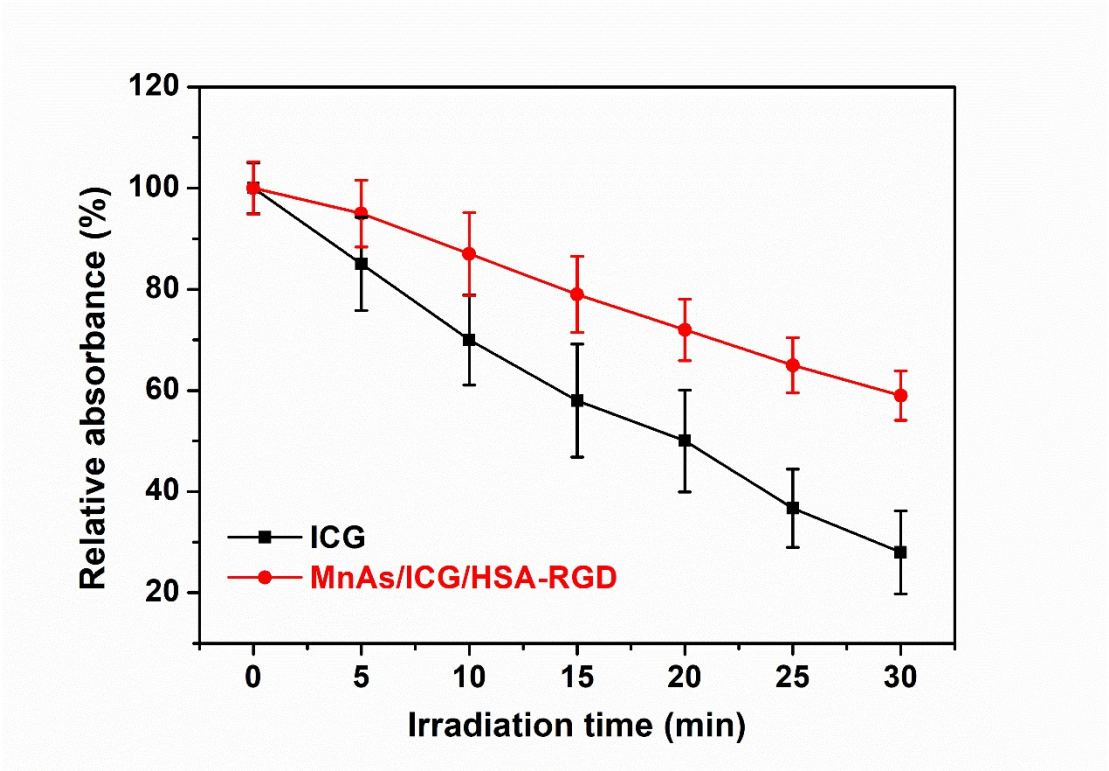

Figure S16. Photostability analysis (relative absorbance) of ICG and MnAs/ICG/HSA-RGD NPs after 808 nm laser irradiation (1 W cm^{-2}) for different periods of time.

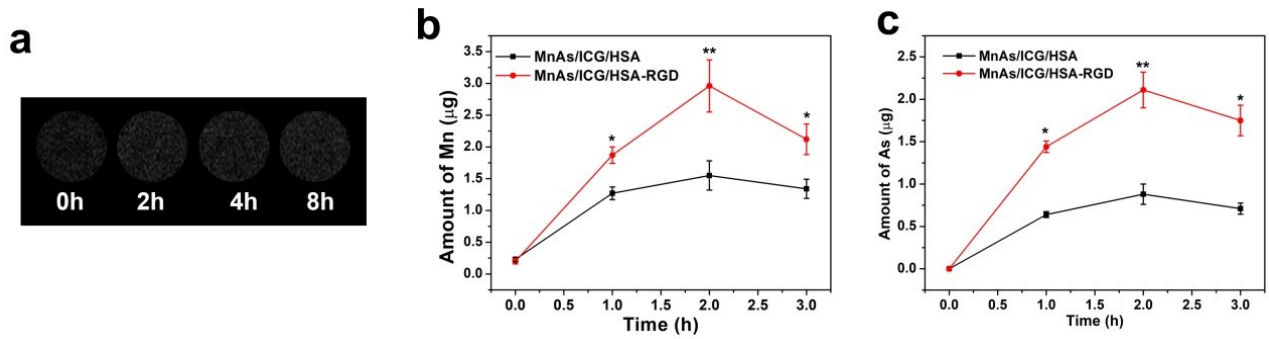

Figure S17. (a) ^{1}H MRI phantom images of MnAs/ICG/HSA-RGD (Mn: 0.4 mM) incubated in 1×PBS buffer (pH 7.4) for different times. Cellular uptakes of (b) Mn and (c) As in SMMC-7721 cells (2×10^{6}) treated as MnAs/ICG/HSA and MnAs/ICG/HAS-RGD(n = 3/group), measured by ICP-MS.

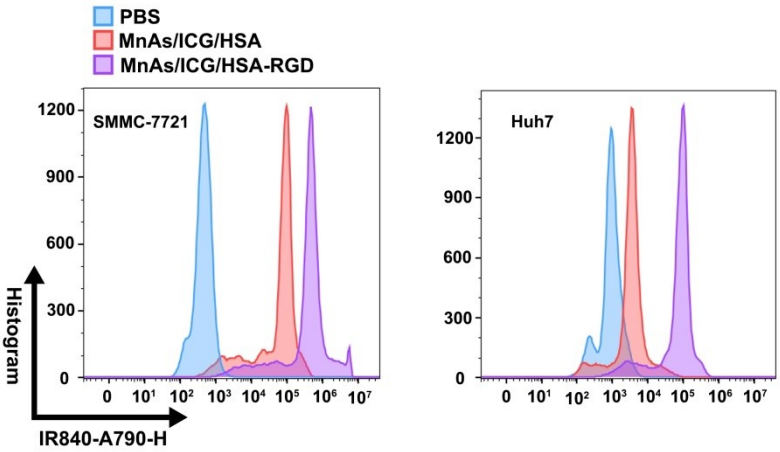

Figure S18. Cellular uptakes of various drugs in SMMC-7721 cells (left) or Huh7 cells (right) after 2 h incubation, evaluated *via* flow cytometry.

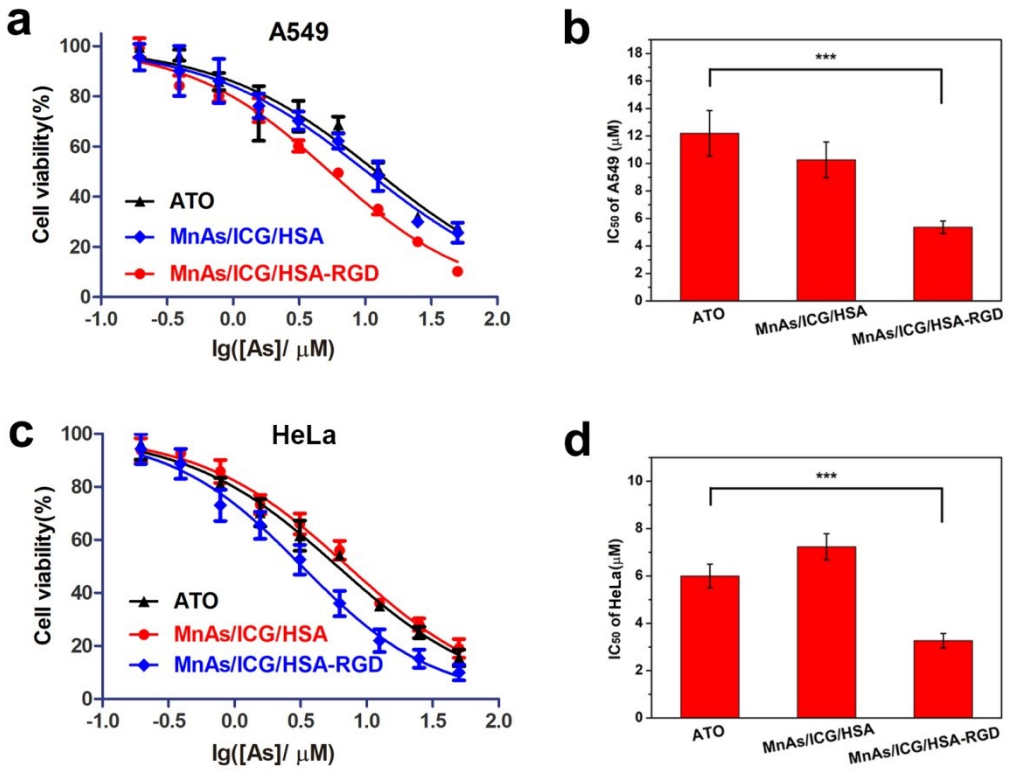

Figure S19. Cytotoxicity of different NP formulas treated with A549 cells (a) and HeLa cells (c), assessed *via* MTT assays. (b) and (d) are IC_{50} values corresponding to (a) and (c). *** indicates $p<0.001$.

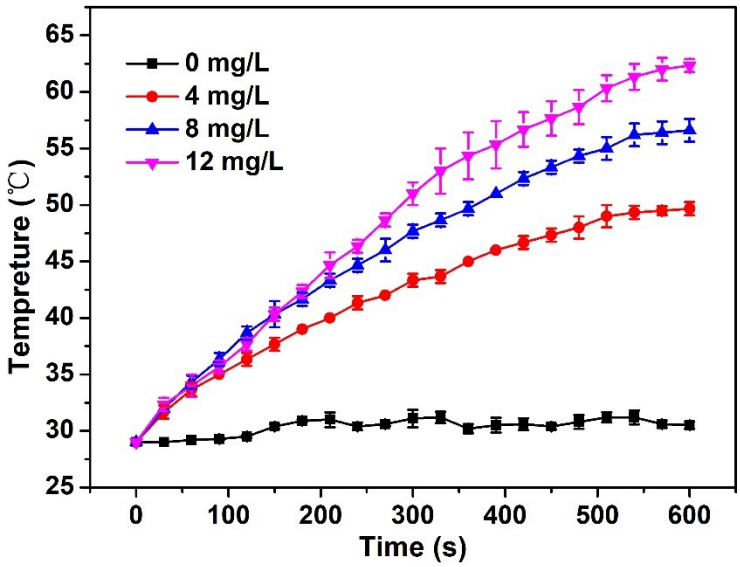

Figure S20. The temperature changes of MnAs/ICG/HSA-RGD with various concentration in irradiated with 808 nm laser (1 W cm^{-2}).

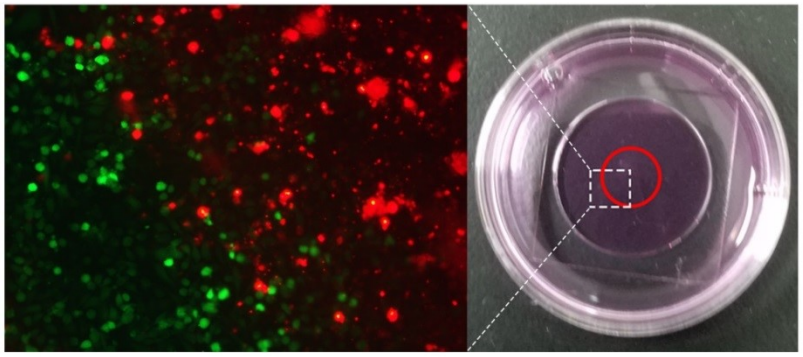

Figure S21. The PTT effect of MnAs/ICG/HSA-RGD on SMMC-7721 cells. A fluorescence microscopy image (left) of the area indicated by the dot white rectangle in the optical image (right). The cells treated with MnAs/ICG/HSA-RGD for 2 h, subjected to 808 nm laser irradiation, and co-stained with calcein AM (green, for live cells)/PI (red, for dead cells). The area irradiated with 808 nm laser (1 W cm^{-2}) is indicated with the red circle.

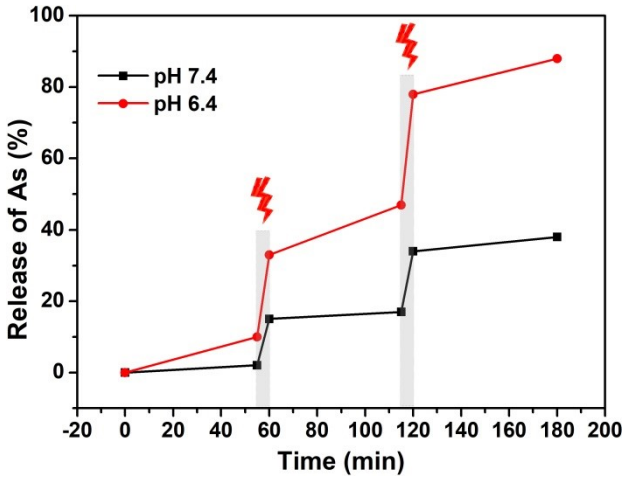

Figure S22. Release profiles of MnAs/ICG/HSA-RGD in 1×PBS buffers at different pH. The solutions were irradiated with 808 nm laser (1 W cm^{-2}) for 5 min at different time points as indicated by red lightning symbols and gray rectangles.

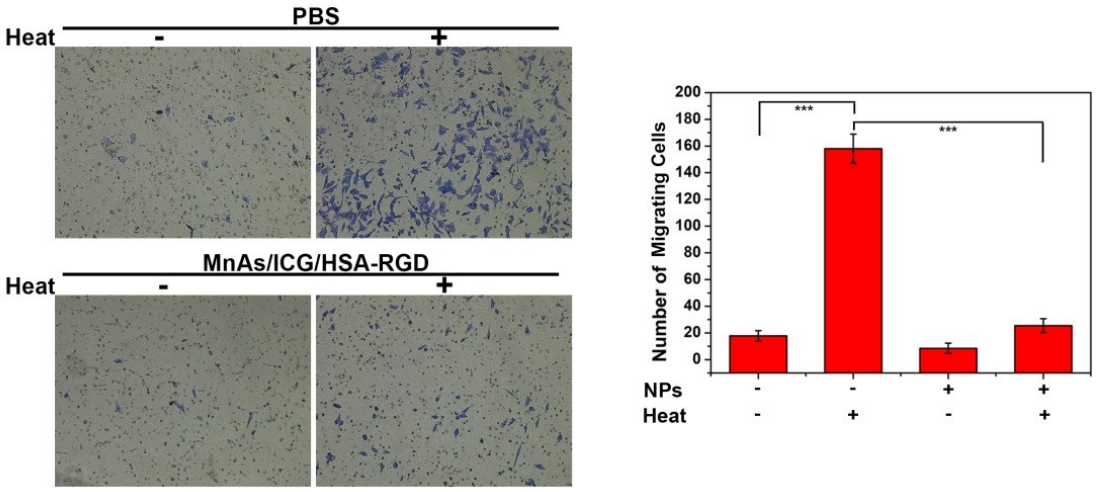

Figure 23. Cell migration assays. Left: optical images of SMMC-7721 cells treated with MnAs/ICG/HSA-RGD NPs or 1×PBS. Preheating was conducted in 45 °C water bath for 10 min. Cells were stained with crystal violet. Right: the corresponding quantitative analysis. *** indicates $p < 0.001$.

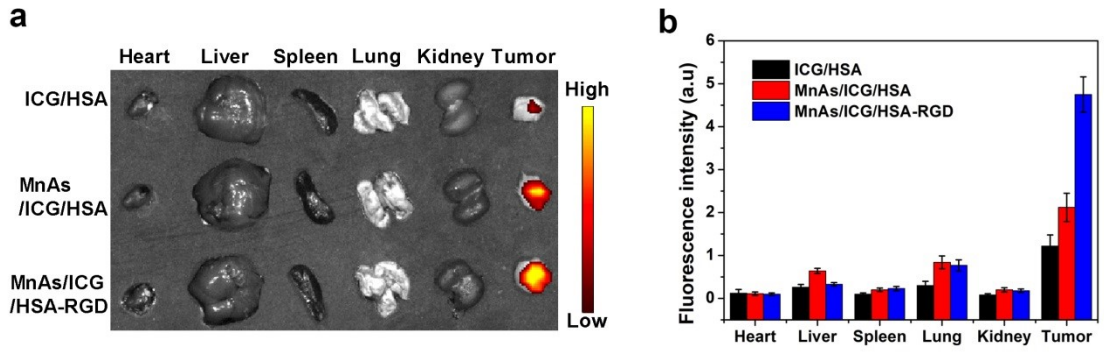

Figure S24. (a) *Ex vivo* fluorescence images of tumors and main organs collected from nude mice bearing SMMC-7721 tumors at 36 h after different treatments as indicated. (b) Semi-quantitative analysis on fluorescence intensities of the tumors and main organs in (a).

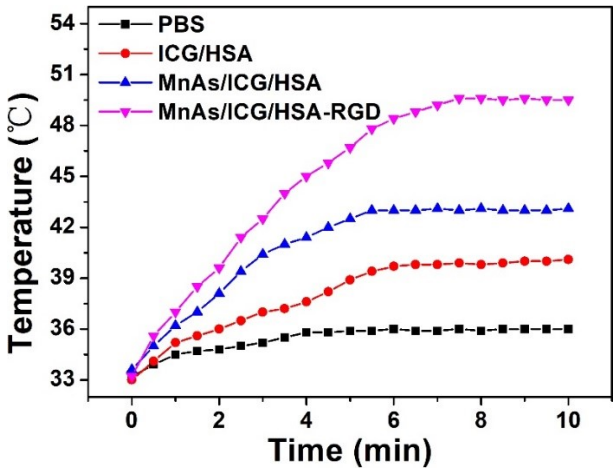

Figure S25. Quantitative analysis of the temperatures recorded during the irradiation process.

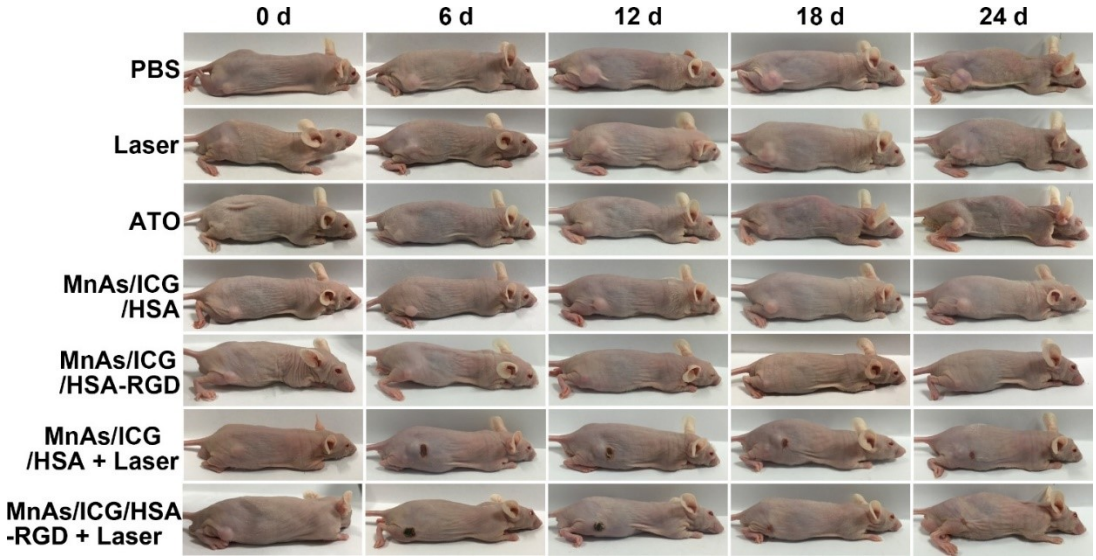

Figure S26. Representative digital photographs of SMMC-7721 tumor-bearing BALB/c nude mice from different groups at various time points.